PHILOSOPHICAL TRANSACTIONS A

Phil. Trans. R. Soc. A.
doi:10.1098/not yet assigned

Sound generation due to the interaction of turbulence with surfaces embedded in transversely sheared flow

M. E. Goldstein[1], S. J. Leib[2] & M. Z. Afsar[3]

[1]*National Aeronautics and Space Administration, Glenn Research Centre, Cleveland OH 44135, USA*
[2]*Ohio Aerospace Institute, Cleveland, OH 44142 USA*
[3]*Strathclyde University, Department of Mechanical and Aerospace Engineering, 75 Montrose St. Glasgow, GI 1XJ*

Keywords: Aeroacoustics, Rapid distortion Theory, Installation effects

Summary

This paper reviews the application of Rapid Distortion Theory (RDT) on transversely shear mean flows to the prediction of sound generated from solid surfaces imbedded in turbulent shear flows. This phenomenon is relevant to the so-called installation noise problem which has received considerable attention in recent years. A few representative results from applications that have appeared in the literature are also presented.

1. Introduction

The focus of this paper is on the use of Rapid Distortion Theory (RDT) to predict the sound generated from solid surfaces imbedded in turbulent shear flows--a phenomenon that is relevant to the so-called installation noise, which has received considerable attention in recent years.

RDT uses linearized equations to analyse rapid changes in turbulent flows such as those that occur when the flow interacts with solid surfaces. It applies whenever the turbulence intensity is small and the length (or time) scale over which the changes take place is short compared to the length (or time) scale over which the turbulent eddies evolve [1-5]. When interpreted asymptotically, these assumptions imply, among other things, that it is possible to identify a distance that is very (infinitely) large on the scale of the interaction, but still small on the scale over which the turbulent eddies evolve. The assumptions also imply that the resulting flow is inviscid and non-heat conducting and is, therefore, governed by the Linearized Euler Equations, i.e., the Euler

*Author for correspondence (marvin.e.goldstein@nasa.gov).

equations linearized about an arbitrary, usually steady, solution to the nonlinear equations— customarily referred to as the base flow.

A large number of papers [4-7] have used locally homogenous RDT, which is a kind of local high-frequency approximation first introduced by Moffatt [8] to study the turbulent motion on planar shear flows. The local nature of this approximation obviates the need for upstream boundary conditions. More general global solutions can be obtained by using Non-homogeneous RDT, which usually provides a more realistic representation of the turbulent interactions. Hunt [1] used non-homogeneous RDT to study the distortion of turbulence by an irrotational base flow. But his analysis was restricted to incompressible flows. Goldstein [2, 3] introduced a much simpler and more general formulation which accounted for compressibility effects and allowed the inclusion of an acoustic as well as a vortical component of the motion (as in the Kovasznay [9] decomposition). But more importantly, the inclusion of compressibility enabled the application of RDT to the prediction of the radiated sound field produced by the surface interactions. This is the main focus of the current paper, which is primarily concerned with the transversely sheared base flows that provide a good representation of rotational shear flows of current technological interest.

The general theory was developed in a series of papers by Goldstein [3, 10] who showed that the solution to the RDT problem can be expressed in terms of the solutions to an inhomogeneous Rayleigh's equation and two convected quantities that can be specified arbitrarily. Goldstein et al [11, 12] expressed the pressure and transverse velocity fluctuations as the convolution product of the Rayleigh equation Green's function and one of the arbitrary convected quantities, which allowed them to represent the Fourier transforms of these quantities as the product of a space-time Fourier transform of the Green's function and the Fourier transform of the convected quantity. They then used this result to predict the acoustic spectrum of the sound produced by turbulence/solid surface interactions in planar mean flows. The experiments show that these acoustic fields are of low frequency and can therefore be calculated from the low frequency Green's function. Goldstein et al [16] used these findings to extend the analysis of [11, 12] to transversely sheared mean flows of arbitrary cross section. They considered the case where the mean surface velocity was equal to zero so that there was no velocity discontinuity or wake downstream of the trailing edge that could support spatially growing instabilities and showed that the low frequency Green's function is independent of the mean flow velocity profile and is therefore the same as the low frequency limit of the zero-mean flow Green's function which can usually be found by using well known standard techniques.

An important consequence of the disparate length scales is that upstream boundary conditions can be imposed infinitely far upstream in a region where the flow is undisturbed by the interaction. The two arbitrary convected quantities do not decay at upstream infinity and can, therefore, be determined from these conditions. But a major problem with this is that these quantities do not correspond to physically measurable variables and the causal RDT solutions for these variables decay at large upstream distances. Goldstein et al [12] showed that appropriate gradients of these quantities do not decay at upstream infinity, used this finding to relate these latter quantities to the arbitrary convected quantities and thereby developed physically realizable upstream boundary conditions for planar mean flows. Reference [16] extended these results to transversely sheared flows of arbitrary cross section. The present paper reviews these theoretical

developments, presents a few representative results from applications of the theory to the installation noise problem and discusses some additional applications of the theory to various noise generation problems that have appeared in the literature.

2. Basic equations

Goldstein et al [11] show that the pressure fluctuation p' produced at the observation point $\boldsymbol{x}=\{x_1,x_2,x_3\}$ by the interaction of the arbitrary convected disturbance $\tilde{\omega}\left(\tau\quad\quad'U(\boldsymbol{y}_T),\boldsymbol{y}_T\right)$ with solid surfaces embedded in the transversely sheared mean flow $\boldsymbol{v}=\{U(\boldsymbol{y}_T),0,0\}$ of an inviscid, non-heat conducting ideal gas is given by

$$p'(\boldsymbol{x},t)=\int_{-T}^{T}\int_{V}G(\boldsymbol{y},\tau\,|\,\boldsymbol{x},t)\tilde{c}\left(\quad\quad\frac{v_1}{U(\boldsymbol{y}_T)},\boldsymbol{y}_T\right)d\boldsymbol{y}d\tau \tag{2.1}$$

where $\boldsymbol{y}=\{y_1,y_2,y_3\}$ is a Cartesian coordinate system with streamwise and transverse components, y_1 and $\boldsymbol{y}_T=\{y_2,y_3\}$ respectively, $\tilde{\omega}\left(\tau\quad\quad'U(\boldsymbol{y}_T),\boldsymbol{y}_T\right)$ can be specified as an upstream boundary condition and $G(\boldsymbol{y},\tau\,|\,\boldsymbol{x},t)$ denotes the Green's function that satisfies the inhomogeneous Rayleigh equation

$$L\,\mathrm{G}(\boldsymbol{y},\tau\,|\,\boldsymbol{x},t)=\frac{D_0^3}{Dt^3}\delta(\boldsymbol{y}-\boldsymbol{x})\delta(\tau-t) \tag{2.2}$$

where

$$L\equiv\frac{D_0}{D\tau}\left(\frac{\partial}{\partial y_i}c^2\frac{\partial}{\partial y_i}-\frac{D_0^2}{D\tau^2}\right)-2\frac{\partial U}{\partial y_j}\frac{\partial}{\partial y_1}c^2\frac{\partial}{\partial y_j} \tag{2.3}$$

is the Rayleigh operator. The first two arguments of $G(\boldsymbol{y},\tau\,|\,\boldsymbol{x},t)$ represent the independent variables and the second two represent the source variables, T denotes a very large but finite time interval, V is a region of space bounded by cylindrical (i.e., parallel to the mean flow) surface(s) S that can be finite, semi-infinite or infinite in the streamwise direction and $\hat{\boldsymbol{n}}=\{\hat{n}_i\}$ is the unit outward-drawn normal to S. The analysis is somewhat unconventional in that the direct Green's function, G, now plays the role of an adjoint Green's function in the solution for p'. See also [11].

The operators

$$\frac{D_0}{D\tau}\equiv\frac{\partial}{\partial\tau}+U(\boldsymbol{y}_T)\frac{\partial}{\partial y_1},\qquad\frac{D_0}{Dt}\equiv\frac{\partial}{\partial t}+U(\boldsymbol{x}_T)\frac{\partial}{\partial x_1} \tag{2.4}$$

denote the convective derivatives, $c^2=c^2(\boldsymbol{y}_T)$ denotes the mean sound speed and $G(\boldsymbol{y},\tau\,|\,\boldsymbol{x},t)$ satisfies the boundary condition

$$\Gamma(\boldsymbol{y},\tau\,|\,\boldsymbol{x},t)=0\quad\text{for}\,\boldsymbol{y}\in S \tag{2.5}$$

where Γ is determined to within an arbitrary convected quantity by

$$\frac{D_0^2\Gamma(\boldsymbol{y},\tau\,|\,\boldsymbol{x},t)}{D\tau^2}\equiv\hat{n}_j c^2\frac{\partial G(\boldsymbol{y},\tau\,|\,\boldsymbol{x},t)}{\partial y_j}, \tag{2.6}$$

on any solid (impermeable) surfaces S that are present in the flow, along with the jump conditions

$$\Delta[G]=\Delta[\Gamma]=0 \ \text{ for } \ \boldsymbol{y}_T\in S_0 \tag{2.7}$$

across the resulting downstream wakes (or vortex sheets): where S_0 denotes the surfaces of discontinuity and $\Delta[\,\cdot\,]$ denotes the jump in the indicated quantity across these surfaces. The mean velocity profiles can be discontinuous across the wakes which can then support additional spatially growing instability waves that can be generated by imposing a Kutta condition at the trailing edge or suppressed by imposing a boundedness requirement.

Equation(2.1), which can be used to predict the sound generated by turbulence interacting with solid surfaces, is a generalization of the well-known Ffowcs Williams and Hall [13] formula (equation 6 in their paper) for the sound produced by the interaction of turbulence with an edge. A major difference between the present result (equation(2.1)) and the Ffowcs Williams and Hall [13] equation is that mean flow interaction effects are now explicitly accounted for—which is an important consideration at the high Mach numbers of interest in aeronautical applications. But there are even more significant differences between these results because (unlike the present solution) the Ffowcs Williams and Hall formulation cannot be used to predict the source convection velocity, to which the calculations show great sensitivity, and does not account for trailing edge vortex shedding--which is known to have a strong effect on the directivity of the sound field.

The density-weighted transverse velocity perturbation $u_\perp$ is given by

$$u_\perp\equiv\frac{1}{|\nabla U|}\frac{\partial U}{\partial y_i}u_i=\frac{1}{|\nabla U|}\frac{\partial U}{\partial y_i}\tilde{\imath}, \tag{2.8}$$

where

$$\boldsymbol{u}=\{u_1,u_2,u_3\}\equiv\rho\{v_1',v_2',v_3'\} \tag{2.9}$$

denotes the mass flux perturbation with $\rho=\rho(\boldsymbol{y}_T)$ being the mean flow density and

$$\boldsymbol{v}'=\{v_1',v_2',v_3'\} \tag{2.10}$$

being the actual velocity perturbation. The pseudo-density-weighted transverse velocity perturbation $\tilde{\imath}$ is given by

$$\tilde{\imath}=\int_{-T}^{T}\int_{V}G_i(\boldsymbol{y},\tau\,|\,\boldsymbol{x},t)\tilde{\imath}\left(\frac{y_1}{U(\boldsymbol{y}_T)},\boldsymbol{y}_T\right)d\boldsymbol{y}d\tau \ \text{ for } \ i=2,3 \tag{2.11}$$

with $G_i(\boldsymbol{y},\tau\,|\,\boldsymbol{x},t)$ determined in terms of the three-dimensional gradient $\partial G(\boldsymbol{y},\tau\,|\,\boldsymbol{x},t)/\partial x_i$ of $G(\boldsymbol{y},\tau\,|\,\boldsymbol{x},t)$ by

$$\frac{D_0}{Dt}G_i(\boldsymbol{y},\tau\,|\,\boldsymbol{x},t)=-\frac{\partial}{\partial x_i}G(\boldsymbol{y},\tau\,|\,\boldsymbol{x},t), \ \text{ for } i=1,2,3 \tag{2.12}$$

It is often desirable to identify the acoustic and hydrodynamic components of the motion in the aeroacoustic applications referred to above. But, as is well known, it is impossible to unambiguously decompose the unsteady motion on a transversely sheared mean flow into acoustic and hydrodynamic components. We can however require that the hydrodynamic component do not radiate any sound at subsonic Mach numbers, with all the acoustic radiation being accounted for by the remaining non-hydrodynamic component. This can be accomplished by dividing the Rayleigh equation Green's function $G(\boldsymbol{y},\tau\,|\,\boldsymbol{x},t)$ that appears in the solution (2.1) into two components, say

$$G(\boldsymbol{y},\tau\,|\,\boldsymbol{x},t)=G^{(0)}(\boldsymbol{y},\tau\,|\,\boldsymbol{x},t)+G^{(s)}(\boldsymbol{y},\tau\,|\,\boldsymbol{x},t) \tag{2.13}$$

where $G^{(0)}(\boldsymbol{y},\tau\,|\,\boldsymbol{x},t)$ denotes a particular solution of Eq. (2.2) which can either be defined on all space or, be required to satisfy appropriate boundary conditions on a streamwise extension of the bounding surface S that extends from minus to plus infinity in the streamwise direction. This decomposition implies the decomposition

$$G_i(\boldsymbol{y},\tau\,|\,\boldsymbol{x},t)=G_i^{(0)}(\boldsymbol{y},\tau\,|\,\boldsymbol{x},t)+G_i^{(s)}(\boldsymbol{y},\tau\,|\,\boldsymbol{x},t) \tag{2.14}$$

of the Greens function derivative (2.12) and the decomposition

$$p'(\boldsymbol{x},t)=p'^{(0)}(\boldsymbol{x},t)+p'^{(s)}(\boldsymbol{x},t) \tag{2.15}$$

for the pressure fluctuation, where $p'^{(0)}(\boldsymbol{x},t)$, which is given by (2.1) and (2.2) with $G(\boldsymbol{y},\tau\,|\,\boldsymbol{x},t)$ replaced by $G^{(0)}(\boldsymbol{y},\tau\,|\,\boldsymbol{x},t)$, does not produce any acoustic radiation at subsonic Mach numbers and can, therefore, be identified with the hydrodynamic component of the unsteady motion. The 'scattered component' $G^{(s)}(\boldsymbol{y},\tau\,|\,\boldsymbol{x},t)$, satisfies the homogeneous Rayleigh's equation along with appropriate inhomogeneous boundary and jump conditions on the streamwise discontinuous surfaces S and S_0 and the corresponding 'scattered solution' $p'^{(s)}(\boldsymbol{x},t)$ therefore, accounts for all of the acoustic components of the motion.

The decomposition(2.14) implies the decomposition

$$\tilde{i}(\quad,\quad)\;\;\tilde{i}(\quad,\quad)\;\;\tilde{\quad}(\quad,\quad)\qquad 2,3 \tag{2.16}$$

of the transverse density weighted pseudo-velocity perturbation $\tilde{i}(\quad,\quad)$ where $\tilde{i}(\quad,\quad)$ is given by (2.11) with $G_i(\boldsymbol{y},\tau\,|\,\boldsymbol{x},t)$ replaced by $G_i^{(0)}(\boldsymbol{y},\tau\,|\,\boldsymbol{x},t)$.

3. The pressure spectrum

Taking the Fourier transform of equations (2.1), (2.11) and(2.12), using the convolution theorem and noting that G satisfies the inhomogeneous Rayleigh equation (2.2) and, therefore depends on τ and t only in the combination $t-\tau$ shows that

$$\bar{p}'(\boldsymbol{x}:\omega)=(2\pi)^2\int_{A_T} e^{i\omega x_1/U(\boldsymbol{y}_T)}\bar{\bar{G}}\left(\boldsymbol{y}_T\mid\boldsymbol{x}:\omega,\omega/U(\boldsymbol{y}_T)\right)\bar{\Omega}^{(0)}(\boldsymbol{y}_T,\omega)d\boldsymbol{y}_T \tag{3.1}$$

and

$$\bar{\tilde{i}}_{\cdot\,\cdot\,\cdot\,\cdot}=-(2\pi)\int_{A_T} e^{i\omega x_1/U(y_T)}\bar{\bar{G}}_i\left(\boldsymbol{y}_T\mid\boldsymbol{x}:\omega,\omega/U(\boldsymbol{y}_T)\right)\bar{\Omega}^{(0)}(\boldsymbol{y}_T,\omega)d\boldsymbol{y}_T,\quad \text{for } i=2,3 \tag{3.2}$$

where A_T denotes the cross section of the volume V, $\alpha(\boldsymbol{x}:\omega)=\lim_{T\to\infty}\alpha(\boldsymbol{x}:\omega;T)$ for $\alpha=\bar{p}',\bar{u}_i,\bar{\Omega}^{(0)}$

$$\bar{p}'(\boldsymbol{x}:\omega,T)\equiv\frac{1}{2\pi}\int_{-T}^{T} e^{i\omega t}p'(\boldsymbol{x},t)\,dt,\quad \bar{\tilde{i}}_{\cdot\,\cdot\,\cdot\,\cdot}\;\;\frac{1}{2\pi}\int_{-T}^{T}\tilde{\cdot\,\cdot\,\cdot\,\cdot} \tag{3.3}$$

$$\bar{\Omega}^{(0)}(\boldsymbol{y}_T:\omega,T)\equiv\frac{1}{2\pi}\int_{-T}^{T} e^{i\omega z}\tilde{\imath}_{\cdot\,\cdot\,\cdot\,\cdot}\,dz \tag{3.4}$$

and

$$\left(U(\boldsymbol{x}_T)\frac{\partial}{\partial x_1}-i\omega\right)^2\bar{\bar{G}}_i\left(\boldsymbol{y}_T\mid\boldsymbol{x}:\omega,k_1\right)\equiv\frac{\partial}{\partial x_i}\bar{\bar{G}}\left(\boldsymbol{y}_T\mid\boldsymbol{x}:\omega,k_1\right),\ i=2,3 \tag{3.5}$$

where

$$\bar{\bar{G}}\left(\boldsymbol{y}_T\mid\boldsymbol{x};\omega,k_1\right)\equiv\frac{1}{(2\pi)^2}\int_{-\infty}^{\infty}\int_{-\infty}^{\infty} e^{i\left[k_1(y_1-x_1)+\omega(t-\tau)\right]}G\left(\boldsymbol{y},\tau\mid\boldsymbol{x},t\right)d\tau dy_1 \tag{3.6}$$

satisfies the Rayleigh equation

$$\mathcal{L}\bar{\bar{G}}=\omega^2\frac{\delta(\boldsymbol{x}_T-\boldsymbol{y}_T)}{(2\pi)^2} \tag{3.7}$$

and

$$\mathcal{L}\equiv\frac{\partial}{\partial y_j}\frac{c^2}{\left(k_1U/\omega-1\right)^2}\frac{\partial}{\partial y_j}+\omega^2\left[1-\frac{c^2\left(k_1/\omega\right)^2}{\left(k_1U/\omega-1\right)^2}\right]\quad j=2,3 \tag{3.8}$$

is the reduced Rayleigh operator.

Since high Reynolds number turbulent flows are usually time stationary [14] it is reasonable to assume that the source function $\tilde{\imath}_{\cdot\,\cdot\,\cdot\,\cdot}$ is a stationary random function of τ [15] and it follows from equation (2.1) that the pressure fluctuation $p'(t,\boldsymbol{x})$ should also be a function of this type. The main focus in aeroacoustics applications is on computing the pressure spectrum which is then given by [15]

$$I(\boldsymbol{x})\equiv\frac{1}{2\pi}\int_{-\infty}^{\infty} e^{i\omega\tilde{\tau}}\left\langle p'(\boldsymbol{x},t)\,p'(\boldsymbol{x},t+\tilde{\tau}\right\rangle\tilde{\cdot\,\cdot\,\cdot\,\cdot}\;\;\lim_{T\to\infty}\left\{\bar{p}(\boldsymbol{x}:\omega,T)\left[\bar{p}(\boldsymbol{x}:\omega,T)\right]^*/2T\right\} \tag{3.9}$$

where the $\langle\,\cdot\,\rangle$ bracket denotes the time average

$$\left\langle p'(\boldsymbol{x},\tau)\,p'\left(\boldsymbol{x},\tau+\tilde{\ }\right)\right\rangle \underset{T\to\infty}{\ } \frac{1}{2T}\int_{-T}^{T} \tilde{\ } \tag{3.10}$$

Inserting the solution (3.1) into (3.9) shows that

$$I(\boldsymbol{x}) = (2\pi)^2 \times \tag{3.11}$$

$$\int_{A_T}\int_{A_T} e^{i\omega x_1\left[1/U(\boldsymbol{y}_T)-1/U(\tilde{\ }\right.} \mathrm{G}\left(\boldsymbol{y}_T \mid \boldsymbol{x}:\omega,\omega/U(\boldsymbol{y}_T)\right)\bar{\bar{G}}^{*}\left(\tilde{\ }\right.$$

and, therefore, that the pressure spectrum depends on the turbulent fluctuations only through source spectrum

$$S\left(\boldsymbol{y}_T\right|\tilde{\ }\underset{\ }{\ } \frac{1}{2\pi}\int_{-\infty}^{\infty} \tilde{\ }$$

$$= (2\pi)\lim_{T\to\infty}\left\{\bar{\Omega}^{(0)}\left(\boldsymbol{y}_T:\omega,T\right)\left[\bar{\Omega}^{(0)}\left(\tilde{\ }\right.\right.^{*}/2T\right\} \tag{3.12}$$

where $\bar{\Omega}^{(0)}\left(\boldsymbol{y}_T:\omega,T\right)$ is given by(3.4).

4. Upstream Boundary conditions

The decomposition (2.13) implies the decomposition

$$\chi = \chi^{(0)} + \chi^{(s)} \tag{4.1}$$

where the symbol χ is used to denote the Fourier transformed pressure fluctuation $\bar{p}'\left(\boldsymbol{x}:\omega,T\right)$, density weighted velocity perturbation $\bar{\tilde{i}}$) or the reduced Rayleigh equation Green's functions $\bar{\bar{G}}\left(\boldsymbol{y}_T \mid \boldsymbol{x}:\omega,k_1\right)$ and $\bar{\bar{G}}_i\left(\boldsymbol{y}_T \mid \boldsymbol{x}:\omega,k_1\right)$, with the $\bar{\bar{G}}^{(0)}\left(\boldsymbol{y}_T \mid \boldsymbol{x}:\omega,k_1\right)$ component of $\bar{\bar{G}}\left(\boldsymbol{y}_T \mid \boldsymbol{x}:\omega,k_1\right)$ either defined on all space or required to satisfy

$$\frac{\hat{n}_j}{\left[\omega-k_1U\left(\boldsymbol{y}_T\right)\right]^2}\frac{\partial}{\partial y_j}\bar{\bar{G}}^{(0)}\left(\boldsymbol{y}_T \mid \boldsymbol{x}:\omega,k_1\right)=0, \quad \text{for } \boldsymbol{y}_T\in C_T \tag{4.2}$$

(where C_T denotes the bounding curve/curves that generate the doubly infinite surface/surfaces that extend S from $y_1=-\infty$ to $y_1=+\infty$). The streamwise homogeneous Green's functions $\bar{\bar{G}}^{(0)}\left(\boldsymbol{y}_T \mid \boldsymbol{x}:\omega,k_1\right)$ and $\bar{\bar{G}}_i^{(0)}\left(\boldsymbol{y}_T \mid \boldsymbol{x}:\omega,k_1\right)$ will then depend on y_1 and x_1 only in the combination x_1-y_1 and we can, therefore, write

$$\bar{\bar{G}}^{(0)}\left(\boldsymbol{y}_T \mid \boldsymbol{x}:\omega,k_1\right)=\bar{\bar{G}}^{(0)}\left(\boldsymbol{y}_T \mid \boldsymbol{x}_T:\omega,k_1\right), \tag{4.3}$$

$$\bar{\bar{G}}_i^{(0)}\left(\boldsymbol{y}_T \mid \boldsymbol{x}:\omega,k_1\right)=\bar{\bar{G}}_i^{(0)}\left(\boldsymbol{y}_T \mid \boldsymbol{x}_T:\omega,k_1\right). \tag{4.4}$$

Reference [16] shows that

$$\tilde{\iota}^{(0)}\left(\quad\right)\to\frac{1}{x_1^2}\boldsymbol{\mathcal{U}}_i\left(t-x_1/U\left(\boldsymbol{x}_T\right),\boldsymbol{x}_T\right),\ \text{as}\ x_1\to-\infty \tag{4.5}$$

and, therefore, that

$$\bar{\tilde{\iota}}^{(0)}\left(\quad\right)\to\frac{e^{i\omega x_1/U(\boldsymbol{x}_T)}}{x_1^2}\bar{\boldsymbol{\mathcal{U}}}_i\left(\boldsymbol{x}_T,\omega\right),\ \text{for}\ i=2,3\ \ \text{as}\ x_1\to-\infty \tag{4.6}$$

where $\boldsymbol{\mathcal{U}}_i\left(z,\boldsymbol{x}_T\right)$ is a function of the indicated arguments and $\bar{\boldsymbol{\mathcal{U}}}_i^{(0)}\left(\boldsymbol{x}_T,\omega\right)$ is its Fourier transform. Reference [16] also shows that the unknown convected quantity $\tilde{\iota}\left(\quad\right)=U\left(\boldsymbol{y}_T\right),\boldsymbol{y}_T\right)$ can be determined from the transverse hydrodynamic components $u_i^{(0)},\ i=2,3$ of the density-weighted transverse velocity perturbation, $u_i,\ i=2,3$ at upstream infinity by imposing the upstream boundary condition

$$\frac{\partial\tilde{\iota}}{\partial y_1}=\overline{|\nabla U|}\nabla_\perp^2 u_\perp^{(0)}+\mathrm{O}\left(\frac{1}{y_1}\right)\ \text{as}\ y_1\to-\infty$$

$$\to\frac{c^2}{U^4}\frac{\partial U}{\partial y_k}\frac{\partial^2}{\partial\tau^2}\boldsymbol{\mathcal{U}}_k\left(\tau-y_1/U,\boldsymbol{y}_T\right),\ \ \text{as}\ \ y_1\to-\infty, \tag{4.7}$$

where

$$\nabla_\perp^2\equiv\frac{\partial^2}{\partial y_2^2}+\frac{\partial^2}{\partial y_3^2} \tag{4.8}$$

and

$$u_\perp^{(0)}\equiv\frac{\partial U}{\partial y_k}\frac{u_k^{(0)}}{|\nabla U|}. \tag{4.9}$$

And it, therefore, follows from(2.8) that

$$\frac{\partial\tilde{\omega}}{\partial y_1}\to\frac{dU}{U^4}\frac{dU}{du}\frac{\partial^2}{\partial\tau^2}|\nabla u|\boldsymbol{\mathcal{U}}_\perp\left(\tau-y_1/U\left(u\right),\boldsymbol{y}_T\right),\ \text{as}\ \ y_1\to-\infty, \tag{4.10}$$

$$\boldsymbol{\mathcal{U}}_\perp\equiv\frac{\partial u}{\partial y_k}\frac{\boldsymbol{\mathcal{U}}_k}{|\nabla u|} \tag{4.11}$$

when the level surfaces of $U=U\left(u\right)$, say $u\left(\boldsymbol{y}_T\right)=\text{constant}$, are more or less concentric and form an orthogonal coordinate system with some function $v\left(\boldsymbol{y}_T\right)$.The transverse velocity perturbation $u_\perp$ then denotes the velocity component perpendicular to these surfaces.

But equations (3.4), (4.7) and (4.10) imply that $\bar{\Omega}^{(0)}\left(\boldsymbol{y}_T:\omega,T\right)$ is related to the upstream transverse velocity coefficient $\boldsymbol{\mathcal{U}}_\perp\left(\xi,\boldsymbol{y}_T\right)$ (in the, as yet, arbitrary orthogonal curvilinear co-ordinate system $\left\{u,v\right\}\left(\boldsymbol{y}_T\right)$) by

$$\frac{i\omega}{U}\bar{\Omega}^{(0)}\left(\boldsymbol{y}_T:\omega,T\right)\to-\omega^2\frac{c^2}{U^4}\frac{dU}{du}|\nabla u|\bar{\boldsymbol{\mathcal{U}}}_\perp\left(\boldsymbol{y}_T;\omega,T\right) \tag{4.12}$$

where

$$\bar{\boldsymbol{u}}_{\perp}\left(\boldsymbol{y}_T;\omega,T\right)\equiv\frac{1}{2\pi}\int_{-T}^{T}e^{i\omega\xi}\boldsymbol{u}_{\perp}\left(\xi,\boldsymbol{y}_T\right)d\xi. \tag{4.13}$$

5. Modelling of physically realizable source spectrum

The time average

$$\Lambda\left(\boldsymbol{y}_T,\tilde{\ }\ \tilde{\ }\right)=\left\langle \boldsymbol{u}_{\perp}\left(\tau,\boldsymbol{y}_T\right)\boldsymbol{u}_{\perp}\left(\tau+\tilde{\ }\ \tilde{\ }\right)\right\rangle \tag{5.1}$$

of $\boldsymbol{u}_{\perp}\left(\tau-y_1/U\left(\boldsymbol{y}_T\right),\boldsymbol{y}_T\right)$ will exist and be independent of τ when $\boldsymbol{u}_{\perp}$ is a stationary function of τ and hence also of $\tau-y_1/U\left(\boldsymbol{y}_T\right)$ [15]. It therefore follows that

$$\frac{1}{2\pi}\int_{-\infty}^{\infty}\exp i\omega\left(\tilde{\tau}\ \tilde{\ }\ /U\left(\boldsymbol{y}_T\right)\right]\Big)\Big\langle \boldsymbol{u}_{\perp}\left(\tau-y_1/U\left(\boldsymbol{y}_T\right),\boldsymbol{y}_T\right)\times$$

$$\boldsymbol{u}_{\perp}\left(\tau-\tilde{\ }\ \tilde{\ }\right)\Big\rangle d\tau\,d\tilde{\tau}=\lim_{T\to\infty}\frac{\bar{\boldsymbol{u}}_{\perp}\left(\boldsymbol{y}_T;\omega,T\right)\left[\bar{\boldsymbol{u}}_{\perp}\left(\tilde{\ }\right.\right.}{2T}. \tag{5.2}$$

And equations (4.12), (3.12), (4.10) and(5.2) then show that the source spectrum $S\left(\boldsymbol{y}_T|\tilde{\ }\right.$ of the convected quantity $\tilde{\omega}$, is related to the normal velocity-like fluctuation $\boldsymbol{u}_{\perp}\left(\tau-y_1/U\left(u\right),\boldsymbol{y}_T\right)$ by

$$S\left(\boldsymbol{y}_T|\tilde{\ }\right.\quad\frac{\rho^2\left(\boldsymbol{y}_T\right)c^2\left(\tilde{\ }\right)}{U^3\left(u\right)U^3\left(\tilde{\ }\right.}\frac{dU\left(\tilde{\ }\right.}{\tilde{\ }}\left|\nabla u\right|\tilde{\ }\ \tilde{\ }$$

$$\int_{-\infty}^{\infty}\exp\left\{i\omega\left(\tilde{\ }\ \tilde{\ }\right)\right\}\tilde{\ }\ \tilde{\ } \tag{5.3}$$

when the level surfaces of $U=U\left(u\right)$, say $u\left(\boldsymbol{y}_T\right)=\text{constant}$, are more or less concentric and form an orthogonal coordinate system with some function $v\left(\boldsymbol{y}_T\right)$.

But the cross correlation $\Lambda\left(\boldsymbol{y}_T,\tilde{\ }\ \tilde{\ }\right.$ of the upstream normal velocity fluctuation needs to be specified before the source spectrum and therefore pressure spectrum can actually be calculated. Goldstein et al [16] show that an appropriate model for $\Lambda\left(\boldsymbol{y}_T,\tilde{\ }\ \tilde{\ }\right.$ is

$$\Lambda\left(\boldsymbol{y}_T,\tilde{\ }\ \tilde{\ }\right.$$

$$\exp-\sqrt{\left[f\left(\eta_2/l_2,\eta_3/l_3\right)\right]^2+\left\{\tilde{\quad}\quad\tilde{\quad}\quad\tilde{\quad}\quad u\right)\right]\}^2/\tau_0^2} \tag{5.4}$$

where the amplitude $A(\boldsymbol{y}_T)$ is expected to vanish as $\boldsymbol{y}_T \to 0,\infty$, τ_0, l_2, l_3 are constants,

$$\tilde{\quad} \tag{5.5}$$

and

$$\eta_2 \equiv \tilde{\quad}\quad\tilde{\quad} \tag{5.6}$$

And since ρc^2 is constant in transversely sheared flows, equation (27) of reference [27] can be used to show that the spectrum (5.3) of this quantity is given by

$$S\left(u,\tilde{\quad}\right) \left[\frac{dU/du\; dU/d\tilde{\quad}}{U^2(u)\;\; U^2(\tilde{\quad}}\right]$$

$$\frac{1}{2\pi}\int_{-\infty}^{\infty} \exp-\sqrt{\left[f\left(\eta_2/l_2,\eta_3/l_3\right)\right]^2+\left\{\tilde{\quad}\quad\tilde{\quad}\quad\tilde{\quad}\right\}^2}\;\tilde{\quad}$$

$$= l_2^4 A(u,v)\left(\rho_\infty c_\infty^2\right)^2\left[\frac{dU/du}{U^2(u)}\frac{dU/d\tilde{\quad}}{U^2(\tilde{\quad}}\right] \frac{\tau_0 f}{\pi\sqrt{1+\tilde{\quad}}} K_1\left(f\sqrt{1+\tilde{\quad}}\right) \tag{5.7}$$

where K_1 denotes the modified Bessel function of the second kind and $A(u,v), f\left(\eta_2/l_2,\eta_3/l_3\right)$ are arbitrary functions that can be chosen to model the experimental data.

6. Calculating the Green's function

It is of course necessary to determine the Green's function before equation (3.11)can be used to carry out numerical computations.. This must in general be done numerically and the calculations, which tend to be very sensitive to the boundary conditions, frequently require great care-especially when mean flow is discontinuous downstream of the trailing edge and therefor contains shear layers that can support spatially growing instability waves. The Wiener-Hopf technique [29] can often be used to minimize these difficulties, but numerical computations are in most cases still required. Baker and Peake [30] developed efficient numerical algorithms for carrying these out.

However, as noted as noted in the introduction, the sound generated by the solid surface interactions turns out to be of low frequency in most applications of technological interest-which means that the low-frequency Green's function can be used in the calculations. Goldstein et al [12, 16] analyzed the sound produced by the interaction of a jet with the trailing edge of a flat plate. Their analysis was restricted to the case where the mean surface velocity was equal to zero so that there was no velocity discontinuity or wake downstream of the trailing edge that could support spatially growing instabilities and the local trailing edge behaviour was, therefore, similar to the zero mean flow case. They found that the low-frequency Green's functions for this interaction do not involve any instabilities and turn out to be the same as the low-frequency limit of the zero-mean-flow Green's functions, when expressed in terms of the streamwise wavenumber, k_1. The results are still dependent on the mean flow because the Green's function is evaluated at $k_1 = \omega/U(\boldsymbol{y}_T)$ in the final formula.

Goldstein et al [12, 16] used this result it to predict the sound field produced by planar and circular jets, respectively, interacting with the trailing edge of a semi-infinite flat plate and Goldstein et al [16] extended the results to higher frequencies by replacing the low frequency limit of the zero mean flow

Green's function by the zero mean flow Greens function itself and thereby increased the range of frequencies over which noise predictions could be made.

7. Applications of theory to the prediction of noise

Olsen and Boldman [17] measured the sound produced by a round jet interacting with the trailing edge of a flat plate whose leading edge was located inside the nozzle and compared their results with the RDT analysis developed in [3]. They showed that the theory accurately predicted the shape of the radiation pattern and its change with jet velocity and that alternative theories [13], which did not account for the effect of velocity gradients at the noise source (e.g. [18], [19]), did not. (The theory was not complete enough to predict absolute levels at that time.) They concluded that these gradients must be accounted for in order to accurately predict the radiated sound.

Ayton and Peake [20] used an earlier version of the theory developed in [10] to analyze the high frequency sound produced by the interaction of a gust with an airfoil embedded in a turbulent shear flow. They also found that the mean shear had a large effect on the far field directivity. Baker and Peake [21] use the more highly developed version of the theory given in [12] to analyze of the effect of boundary layer shear on trailing edge noise. Baker and Peake [28] extended the theory of reference [3] to slowly varying mean flows.

As noted above reference [12] used further developments of the theory to study the noise produced by the large aspect ratio rectangular jet interacting with the trailing edge of a flat plate shown in figure 1.

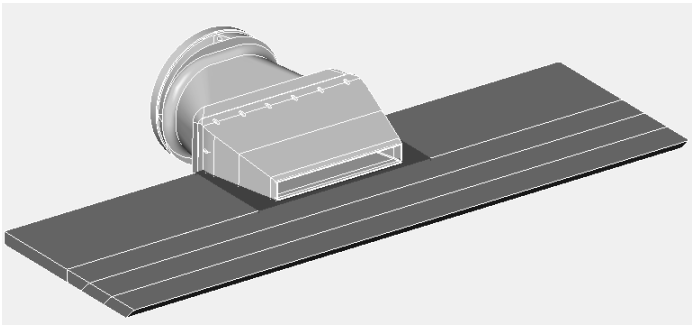

Figure 1 rectangular jet interacting with the trailing edge of a flat plate

They used experimental data to model the turbulence correlation function within the jet and the result was used to calculate the acoustic spectrum. The computations were found to be in excellent agreement with data taken at NASA Glenn research center [22-25]. Comparisons were carried out over a broader range of polar angles and three different Mach numbers. Details of the flow and source models are given in [12].Some typical results are shown in figure 2

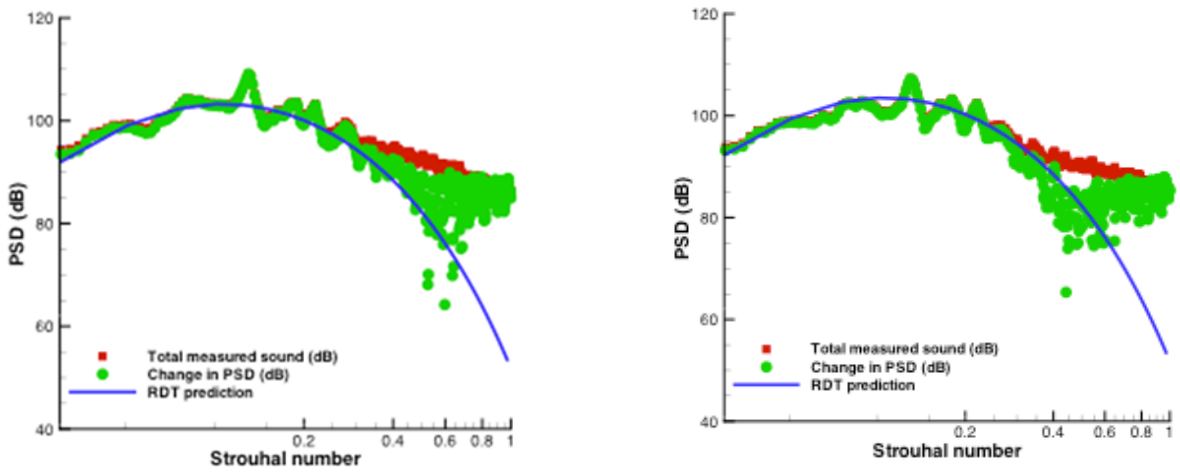

a) b)

Figure 2. Comparisons of RDT solution for planar jet with experimental data of Brown [23] for the power spectral density, PSD, of the far-field pressure fluctuation vs. Strouhal number, St, based on jet exit velocity and equivalent nozzle diameter at polar angles a) $\theta = 95^0$ **and b)** $\theta = 105^0$ **measured from the downstream jet axis. Acoustic Mach number based on jet exit velocity is 0.9. From reference[12].**

Reference [16] used the theory along with the low frequency Green's function to predict the sound field produced by the circular jet interacting with the trailing edge of a semi-infinite flat plate shown in figure 3. But the formulas obtained in that reference are quite general and should apply to many different flow configurations, such as the multiple jet configuration shown in figure 4. Computations were again carried out over a broader range of azimuthal angles and three different Mach numbers. Good agreement was obtained in this case as well. Some typical results are shown in figure 5.

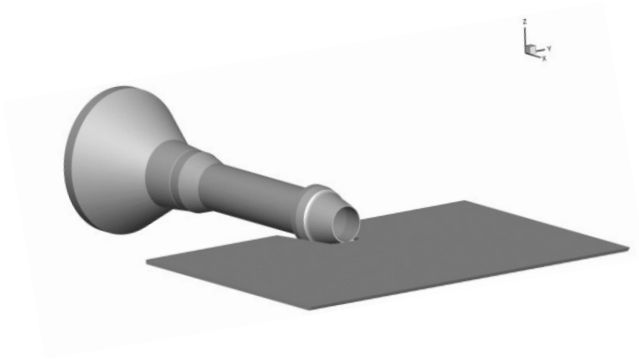

Figure 3 Round jet interacting with the trailing edge of a flat plate

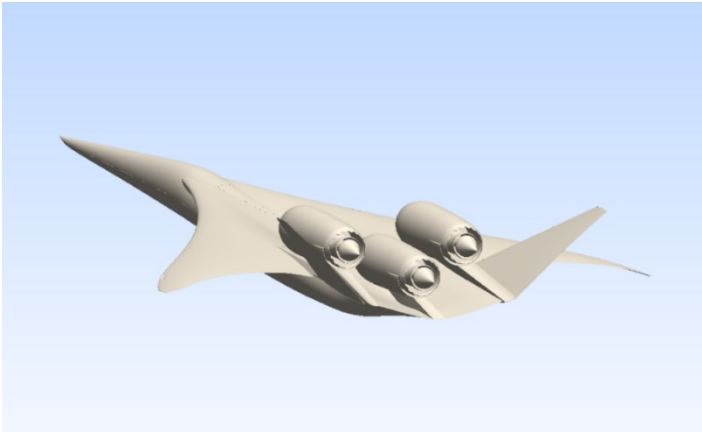

Figure 4 Supersonic cruise concept aircraft with top mounted engines. Ramakrishnan et al NASA CR-2018-219936 [26] (provided by Dr. James Bridges)

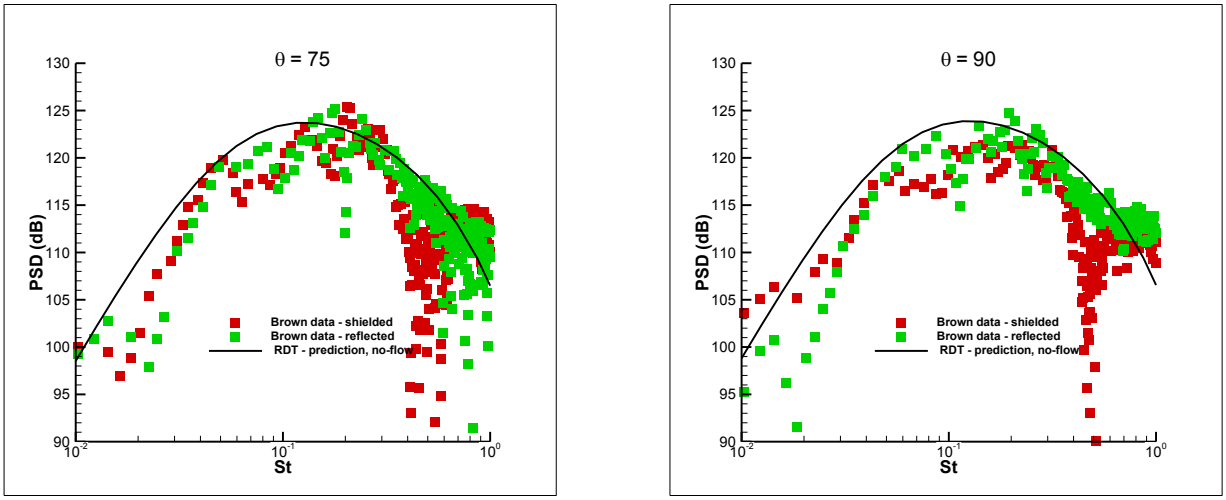

a) b)

Figure 5 - Comparison of composite RDT solution for round jet with experimental data of Brown [23, 24] for the power spectral density, PSD, of the far-field pressure fluctuation vs. Strouhal number, St, based on jet exit velocity and nozzle diameter at polar angles: a) $\theta = 75^0$ **and measured from the downstream jet axis. Acoustic Mach number based on jet exit velocity is 0.9. From reference [16}.**

8. Conclusions

The results described in this paper are applicable to a wide range of flow-surface interaction problems and can be extended to more complicated geometries and surface boundary conditions, such as deformable plates which could be of interest in optimisation studies for reducing edge-generated noise.

It has frequently been argued that instability modes, or more generally coherent structures, are the main source of sound in turbulent shear flows [31]. Relevant theories have been developed for supersonic [32, 34] and subsonic [34, 35] jets. But the instability waves on a parallel mean flow don't actually radiate any

sound at subsonic Mach numbers. It is only the modulation of those waves by viscous and nonlinear processes that actually produce acoustic radiation. The continuous spectrum can also represent the coherent structures. We believe that that this part of the spectrum which has many more components than the discrete modes provides the best representation of the turbulence.

References

1. Hunt, J. C. R. 1973 A theory of turbulent flow around two dimensional bluff bodies J. Fluid Mech. 61:625-706

2. Goldstein, M.E. 1978, unsteady vortical and entropic distortions of potential flows round arbitrary obstacles, J. Fluid Mech. 89:433-468

3. Goldstein, M.E., 1979, Scattering and distortion of the unsteady motion on transversely sheared mean Flows, J. Fluid Mech. Vol.91, part 4, pp. 601-632

4. Sagaut, P. and Cambon, C., 2008, Homogeneous Turbulence Dynamics, Cambridge university Press.

5. Batchelor, G.K. and Proudman, I., 1954, The effect of rapid distortion of a fluid in turbulent motion, Quarterly Journal of Mechanics and Applied Mathematics, Vol. 7, No. 1 pp. 83 – 103.

6. Taylor, G.I., 1938, The spectrum of turbulence, Proc. R. Soc. A 164, pp.476-490.

7. Xie, Z., Karimi, M. & Girimaji, S. S. 2017, Small perturbation evolution in compressible Poiseulle flow-velocity interactions and obliqueness effects, *Journal of Fluid Mech.* 814 pp. 249-276

8. Moffatt, H.K., 1976, interaction of turbulence with strong wind shear. In colloquium on atmospheric turbulence and radio wave propagation (ed. A. M. Yaglom and V. I.Tatarski). pp. 139-156. Nauka

9. Kovasznay, L. S. G., 1953, Turbulence in supersonic flow, J. Aero Sci. 20, issue number 10pp. 657-674.

10. Goldstein, M.E., 1978, Characteristics of the unsteady motion on transversely sheared mean Flows, J. Fluid Mech. Vol.84, part 2, pp. 305-329

11. Goldstein, M.E., Afsar, M. Z. and Leib, 2013, Non-homogeneous rapid distortion theory on transversely sheared mean flows, J. Fluid Mech. Vol.736, pp. 532-569

12. Goldstein, M.E., Leib, S. J. and Afsar, M. Z. 2017, Generalized rapid distortion theory on transversely sheared mean flows with physically realizable upstream boundary conditions: application to the trailing edge problem, J. Fluid Mech. Vol.824, pp. 477-512

13. Ffowcs Williams, J. E. and Hall, L. H., 1970, Aerodynamic sound generation by turbulent flow in the vicinity of a scattering half plane, J. Fluid Mech., 40, 657-670

14. Pope, S., 2000, *Turbulent Flows*, 1st Edition, Cambridge University Press.

15. Weiner, N. 1938, The use of statistical theory to study turbulence, Proc.5th Int. Congress Appl. Mech. P.356-360

16. Goldstein, M. E., Leib, S. J. & Afsar, M. Z. 2019, Rapid distortion theory on transversely sheared mean flows of arbitrary cross section, submitted to J. Fluid Mech.

17. Olsen, W. & Boldman, D., 1979, Trailing edge noise data with comparison to theory. AIAA paper # 1979-1524, AIAA 12th Fluids and Plasma Dynamics Conference
18. Amiet, R. K., 1975, Acoustic radiation from an Airfoil in a turbulent stream, Journal of sound and Vibration, Vol. 81, pp407-420
19. Paterson, R. W., and Amiet, R. K., 1976, Acoustic radiation and surface pressure characteristics of an Airfoil due to incident turbulence, AIAA paper #76-571, AIAA Aeroacoustics Conference, Palo Alto CA., July 20-23
20. Ayton, L.J. and Peake, N, 2014, An analytic approach to high-frequency gust-aerofoil interaction noise in steady shear flows,' AIAA 2014-2322.
21. Baker, D. I. and Peake, N., 2017, Effect of boundary-layer shear on trailing edge noise, 23rd AIAA/ACEAS Aeroacoustics conference Paper # AIAA-2017-3169.
22. Bridges, J., Brown, C.A. and Bozak, R., 'Experiments on Exhaust of Tightly Integrated Propulsion Systems,' AIAA paper #2014-2904.
23. Brown, C. A., 2015, An Empirical Jet-Surface Interaction Noise Model with Temperature and Nozzle Aspect Ratio Effects, *53rd AIAA Aerospace Sciences Meeting*.
24. Brown, C., 2012 Jet-Surface Interaction Test: Far-Field Noise Results, ASME Paper GT2012-69639.
25. Bridges, J., 2014, Noise from Aft Deck Exhaust Nozzles—Differences in Experimental Embodiments *52nd AIAA Aerospace Sciences Meeting – 13-17 January 2014, Nat'l Harbor, MD*
26. Ramakrishnan, K., Paliath, U., Pastouchencko, N., Malcevic, I., Pilon, A., Morgenstern, J., Buonanno, M., Martinez, M., Majjigi, M.2018, Evaluation of Low Noise Integration Concepts and Propulsion Technologies for Future Supersonic Civil Transports NASA CR-2018-219936
27. Leib, S.J. and Goldstein, M.E., 2011 "Hybrid Source Model for Predicting High-Speed Jet Noise," *AIAA Journal*, Vol. 49, No. 7
28. Baker, D. I. and Peake, N., 2018, 'Trailing-edge noise in slowly-varying, sheared flow,' AIAA paper# 2018-2810.
29. Noble, B. 1958, *Methods Based on the Wiener-Hopf Technique for the Solution of Partial Differential Equations*. Pergamon.
30. Baker. D. J. and Peake, N. Scattering on rotational flows. 25th AIAA/ACEAS Aeroacoustics conference Paper # AIAA-2019-2554.
31. Jordan. P. & Colonius. T., 2013, Wave Packets and Turbulent Jet Noise, Annual. Rev. Fluid Mech., Vol. 45, pp. 173-195. https://doi.org/10.1146/annurev-fluid-011212-140756
32. Tam, C. K. W. and Burton, D. E., 1984, Sound generated by instability waves of supersonic flows. Part 2. Axisymmetric jets, Journal of Fluid Mechanics, Vol. 138, pp. 273-95. https://doi.org/10.1017/S0022112084000124
33. Wu, X. 2005, Mach wave radiation of nonlinearly evolving supersonic instability modes in shear layers , Journal of Fluid Mech., Vol 523, pp. 121-159. https://doi.org/10.1017/S0022112004002034

34. Sihna, A., Rodriguez, D., Guillaume, G. . and Colonius, T., 2014, Wavepacket models for supersonic jet noise, Journal of Fluid Mech., Vol 742, pp. 71-95. https://doi.org/10.1017/jfm.2013.660

34. Wu, X. & Huerre. P., 2009, Low-frequency sound radiated by a nonlinearly modulated wavepacket of helical modes on a subsonic circular jet, Journal of Fluid Mech., Vol 637, pp. 173-211. https://doi.org/10.1017/S0022112009990577

35. Cavalieri, A. V. G and Agarwal, A., 2014, Coherence decay and its impact on sound radiation by wavepackets Journal of Fluid Mech., Vol 748, pp. 399-415. https://doi.org/10.1017/jfm.2014.186

Additional Information

Acknowledgments The authors would like to thank Dr. James Bridges for providing the photograph in figure 4 and Dr Clifford Brown for providing his experimental data and helpful discussions on the interpretation.

Funding Statement

This work was supported by the NASA Advanced Air Vehicle Program, Commercial Supersonic Technology (CST) and Advanced Air Transport Technology (AATT) Projects. MZA would like to thank Strathclyde University for financial support from the Chancellor's Fellowship